Vision, Modeling, and Visualization (2015)
D. Bommes, T. Ritschel, and T. Schultz (Eds.)

Light Field Imaging through Household Optics

A. Wender[1], J. Iseringhausen[2], B. Goldlücke[3], M. Fuchs[1], M. B. Hullin[2]

[1]University of Stuttgart, Germany [2]University of Bonn, Germany [3]University of Konstanz, Germany

In this supplemental file, we document a larger set of results and the full resolution (JPEG-compressed to save on file size) input pictures used. The complete data set consists of four different light field transformers, two refractive and two reflective types.

- cathedral glass quite randomly structured surface
- cross-ribbed glass regular structure of lenslet like components
- mirroring spheres small glass spheres from seasonal ornament with a wide field of view
- kitchen spoons 18/10 stainless steel spoon of two different sizes

Figures 1 to 4 show results for each transformer types. Unless otherwise stated, the renderings are made from the 99% most consistent rays observed.

The results of our consistency assessment in the different light fields is shown in Figure 5.

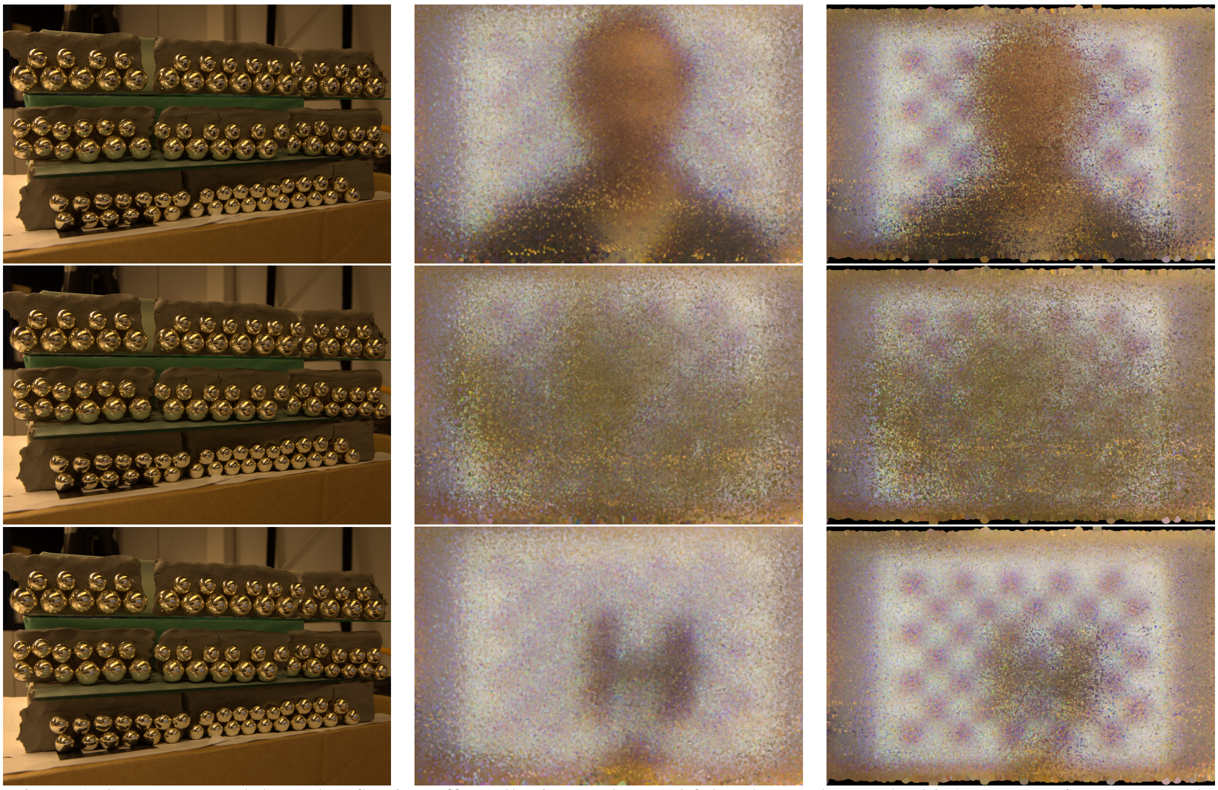

Figure 1: Scene captured through reflection off small mirror spheres. Of the observed rays, the 30% most consistent are used.

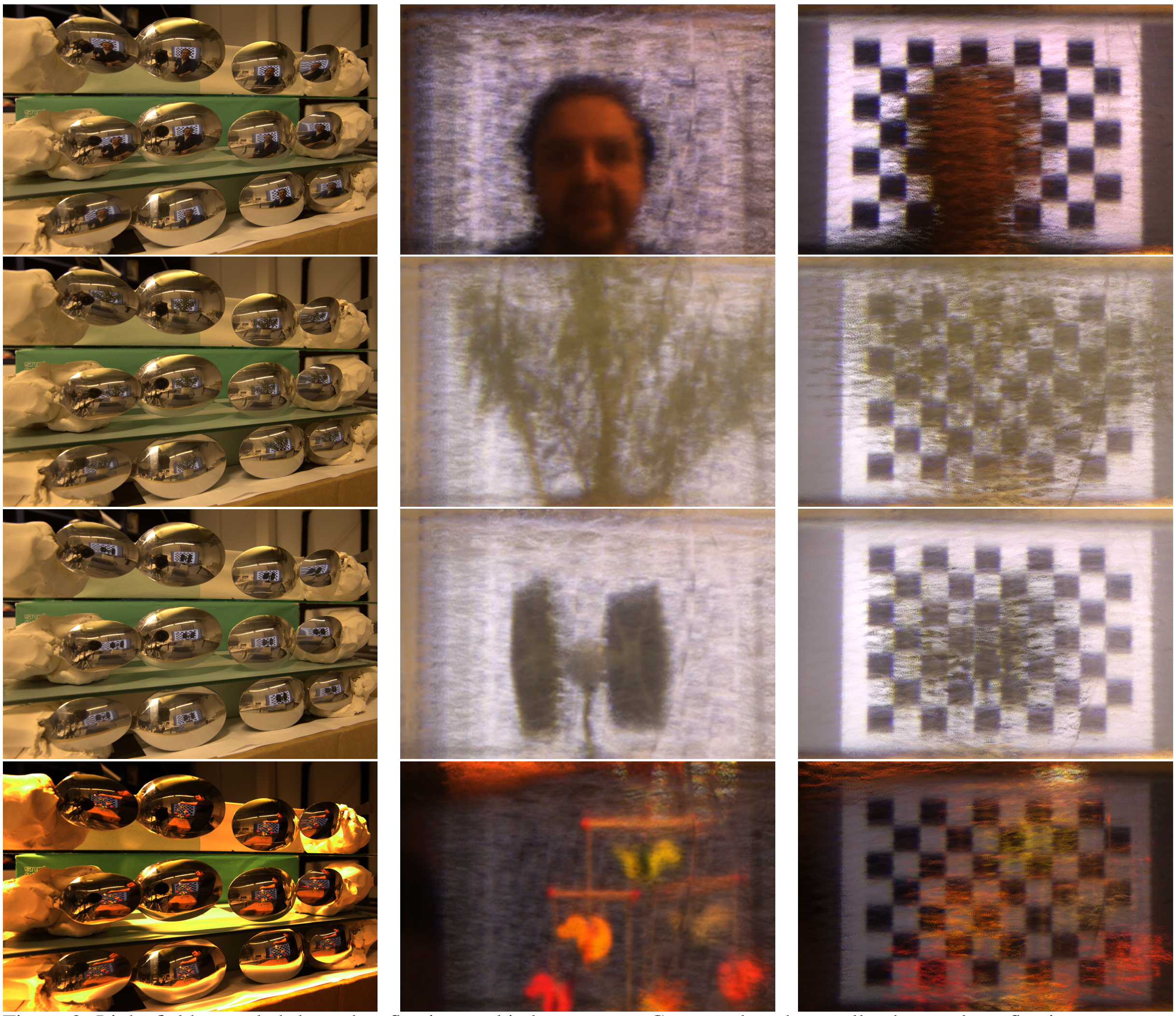

Figure 2: Light field recorded through reflection on kitchen spoons. Compared to the small spheres, the reflecting geometry provides a smaller, but still sufficient field of view, increasing the reconstruction quality.

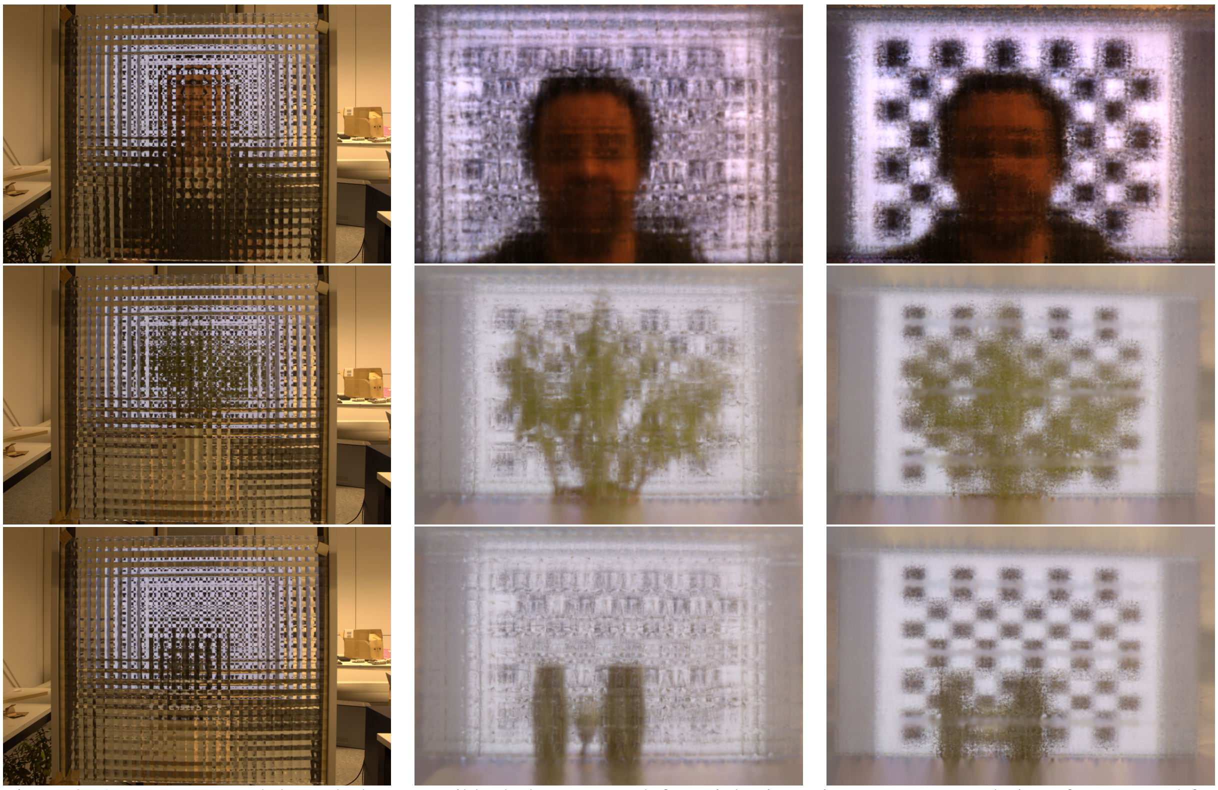

Figure 3: A scene captured through the cross-ribbed glass. From left to right: input image output renderings for near and far focal planes. This setup resembles conventional integral photography through many lenslet arrays. The input picture shown is cropped to the size of the transformer.

Figure 4: A scene captured through cathedral-type glass. From left to right: input image output renderings for near and far focal planes. Due to the quasi-random scrambling of the incoming rays, we can find reasonable rays for almost all ray required ray directions. Accordingly, we obtain comparably little distortion for out-of-focus planes.

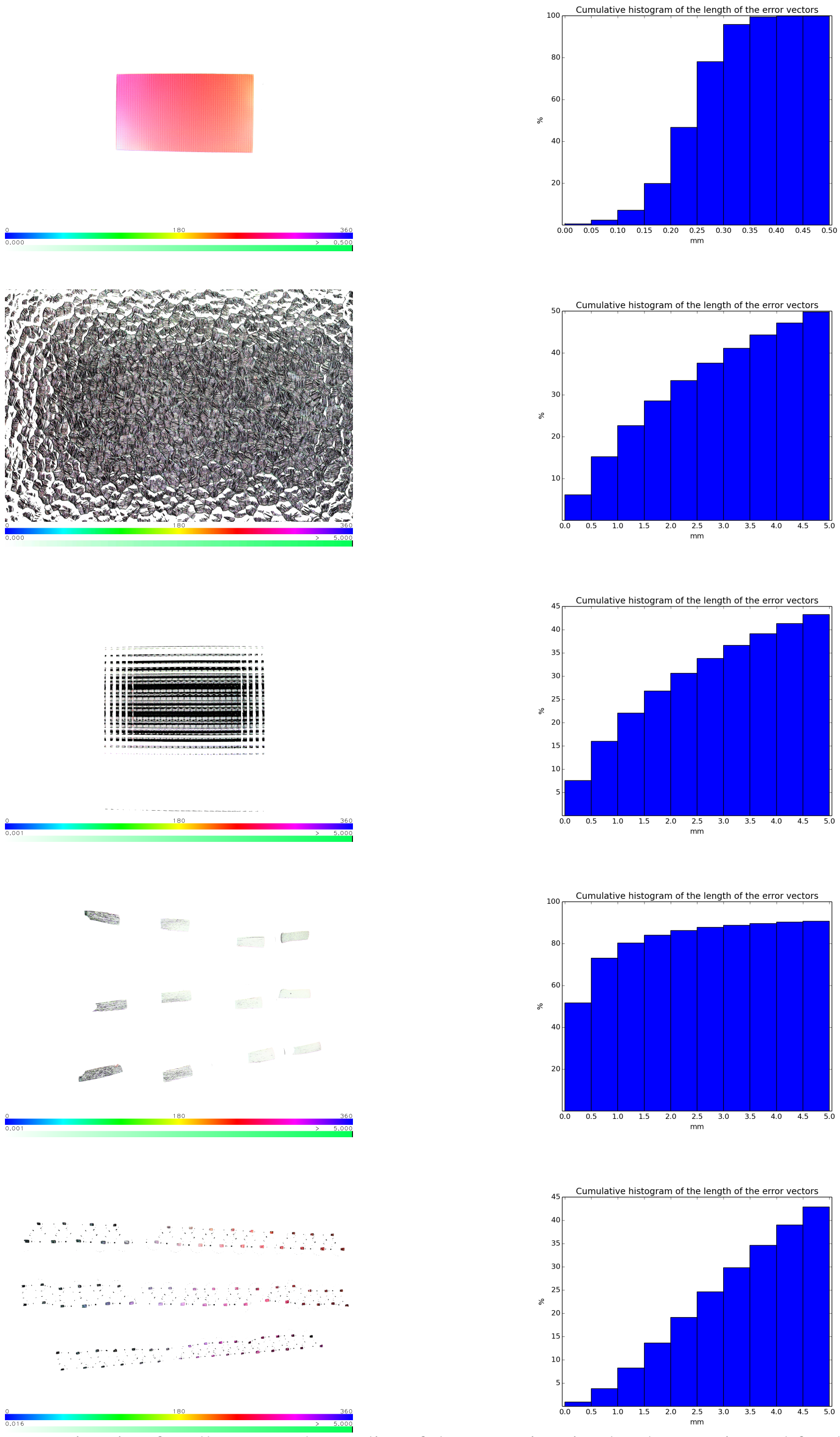

Figure 5: Consistency estimation for all setups. The quality of the ray estimation has been estimated for the absence of a light field transformer (first row) and for cathedral, cross-ribbed glass, kitchen spoons and the small spheres (second to last row). Each ray is calculated as a least-squares line fit through measured points on three calibrated screen positions. We calculate an error vector $\mathbf{e}(\mathbf{r})$ between the measured point on the middle screen position, and the intersection point of this screen and a line connecting the measured points of the nearest and most distance screen position, see section 3.1 in the paper. The left column pictures show the orientation and the magnitude of the $\mathbf{e}$. The direction is color coded, while the magnitude is saturation coded. Error vector lengths above a dataset dependent threshold are marked black. The right columns shows an cumulative histogram of the length of the error vectors. For reference, the pixel pitch on the screen used for calibration is 0.3 mm.